JOURNAL OF AIRCRAFT
Vol. 39, No. 3, May–June 2002

# Apparent Mass of Parafoils with Spanwise Camber

Timothy M. Barrows*
*Charles Stark Draper Laboratory, Inc., Cambridge, Massachusetts 01239*

**For an arbitrarily shaped body, there may be more than one center of apparent mass. The apparent mass of a parafoil shape for motions along various axes is computed using potential flow analysis. From this, the 6 × 6 apparent mass matrix about some reference point is computed. Parametric forms for estimating the terms are given. The existence of multiple mass centers results in off-diagonal terms in this matrix that couple the translational and rotational motions. It is shown how the nondiagonal 6 × 6 apparent inertia matrix about a certain reference point can be used to compute the corresponding apparent mass matrix at any other reference point. Dynamic equations including nonlinear terms are presented.**

## Nomenclature

$\boldsymbol{A}_{oa}$ = apparent inertia matrix about $O$
$\boldsymbol{A}_{oR}$ = real mass inertia matrix about $O$
AR = aspect ratio
$\boldsymbol{a}_{ab}$ = vector to $a$ from $b$
$b$ = span
$c$ = chord
$\boldsymbol{D}$ = $\boldsymbol{a}_{ro}^{\times} + \boldsymbol{a}_{pr}^{\times}\boldsymbol{S}_2$
$\boldsymbol{e}_n$ = elementary unit vector along axis $n$
$\boldsymbol{f}$ = force
$\boldsymbol{f}_{\text{aero}}$ = aerodynamic force
$\boldsymbol{f}_{a\,\text{nl}}$ = apparent mass nonlinear force
$\boldsymbol{f}_e$ = external (nonaerodynamic) force
$\boldsymbol{f}_{R\,\text{nl}}$ = real mass nonlinear force
$\boldsymbol{g}$ = torque
$h$ = arch height, Fig. 5
$\boldsymbol{h}_o$ = angular momentum about $O$
$h^*$ = $h/b$
$\boldsymbol{I}$ = principle axis inertia matrix, Eq. (17)
$I$ = identity matrix
$\boldsymbol{J}_o$ = inertia matrix about $O$, rotational part
$K$ = Bateman coefficient
$k_A$, $k_B$ = three-dimensional correction factors
$l$ = perimeter of maximum cross section normal to flow
$\boldsymbol{M}$ = apparent inertia matrix, translational part
$m_{ii}$ = scalar component of $\boldsymbol{M}$
$m_R$ = solid mass plus enclosed air mass
$O$ = origin of coordinate frame, Fig. 2
$\boldsymbol{p}$ = linear momentum vector
$\boldsymbol{p}_R$ = momentum of the real mass
$\boldsymbol{p}_t$ = total momentum
$\boldsymbol{Q}$ = $\boldsymbol{S}_2\boldsymbol{a}_{pr}^{\times}\boldsymbol{M}\boldsymbol{a}_{ro}^{\times}$
$R$ = radius of parafoil, Fig. 5
$\boldsymbol{r}$ = vector from the origin $O$ to the center of real mass
$S$ = planform area
$\boldsymbol{S}_n$ = selection matrix, Eq. (14)
$T$ = kinetic energy
$t$ = wing thickness ratio
$\boldsymbol{v}_o$ = velocity of point $O$
$\boldsymbol{\omega}$ = angular velocity

*Subscripts*

$a$ = apparent mass or inertia
$c$ = confluence point
cen = centroid
$f$ = flat (uncambered) wing
MC = motion center
nl = nonlinear
$o$ = origin of coordinate frame, Fig. 2.
$p$ = pitch center
$R$ = real mass or inertia
$r$ = roll center

## Introduction

A PARAFOIL is a very light structure that is strongly influenced by the apparent mass effects of the surrounding air. The subject is discussed by Lissaman and Brown,[1] who model the parafoil as an ellipsoid. Brown[2] provides a discussion of the increasing effect of apparent mass on parafoil turning performance as the scale gets larger. The theoretical basis for the notion of apparent mass is provided by Lamb.[3] A more recent derivation using modern terminology is given in Ref. 4. Thomasson[5] provides a general analysis in which the fluid medium may have velocity gradients or accelerations.

Although it is tangential to the dynamics of the parafoil, note that there is a substantial body of literature on the apparent mass of cupped parachutes. Yavuz[6] provides some discussion of previous literature, along with experimental data showing that a potential flow analysis does not provide accurate estimates of the apparent mass of a cupped parachute because of the large amount of separated flow. In Refs. 7–11 there is additional background. Another, indirectly related article, is that by Ioselevskii,[12] who computes lift, drag, and side force on an arched wing using lifting line theory.

The Charles Stark Draper Laboratory, Inc., conducted an investigation sponsored by the U.S. Army Natick Laboratory on a Precision Guidance Airdrop System using ram-air parafoils. As part of this program, flight tests were conducted at NASA Dryden Flight Research Center. An engineering simulation was also implemented at Charles Stark Draper Laboratory, Inc., that includes parafoil and environment models. In the process of comparing simulation results to parafoil flight data, it was determined that existing attempts to model parafoil apparent mass effects using an ellipsoid must be modified to reproduce the correct turning dynamics. That is the motivation for the present study.

The problem is identifying the center of mass. Almost all studies of apparent mass effects focus on either an ellipsoid, a two-dimensional shape, or an axisymmetric body. An ellipsoid enjoys the virtue of having three planes of symmetry and a geometric centroid that is at the intersection of all three planes. A single center of apparent mass can, therefore, be found that is, not surprisingly, at the centroid. Similarly, when there is axisymmetry, the center of

Presented as Paper 2001-2006 at the 16th Aerodynamic Decelerator Systems Conference, Boston, MA, 21–24 May 2001; received 15 August 2001; revision received 4 March 2002; accepted for publication 7 March 2002. Copyright © 2002 by Timothy M. Barrows. Published by the American Institute of Aeronautics and Astronautics, Inc., with permission. Copies of this paper may be made for personal or internal use, on condition that the copier pay the $10.00 per-copy fee to the Copyright Clearance Center, Inc., 222 Rosewood Drive, Danvers, MA 01923; include the code 0021-8669/02 $10.00 in correspondence with the CCC.

*Principal Member Technical Staff, Vehicle Systems Group. Senior Member AIAA.

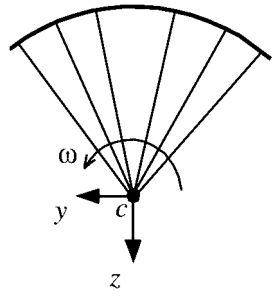


**Fig. 1 Parafoil of zero thickness, front view.**

apparent mass must lie along the centerline, and it turns out that in this case a single apparent mass center can also be found that is at the volumetric centroid. In the more general case, it may not be possible to find a single point at which the rotational and translational motions are decoupled.

One property of the center of mass is that, for rotation about this point, there is less resistance to rotational acceleration, that is, lower moment of inertia, than for rotation about any other fixed point. Consider the hypothetical parafoil shown in Fig. 1, consisting of a wing of zero thickness with circular arc spanwise camber. The confluence point of the support lines is at the center of the circular arc. If this wing rolls about the confluence point, it will not cause any disturbance to the surrounding fluid, because of the lack of thickness. The apparent moment of inertia is, thus, zero, which must be a minimum because negative moments of inertia are physically impossible. Thus, the confluence point is the center of apparent mass for rotation about the $x$ axis. However, if we rotate about an axis parallel to the $y$ axis and the wing does not have any chordwise camber, the center of apparent mass is not at the confluence point but at some higher point, closer to the wing. In fact, if it is further hypothesized that the chordwise camber is negative, it is even possible for the center to be above the wing for rotation about an axis parallel to the $y$ axis. The conclusion is inescapable that this wing has at least two centers, one for rotation in the $y$–$z$ plane and one for rotation in the $x$–$z$ plane.

The present paper examines the case in which there are only two planes of symmetry, such that the parafoil has lateral symmetry and fore-and-aft symmetry, but the top half is not the same as the bottom half. Therefore, for each of the three axes of motion, what we have been calling the center must lie somewhere on the intersection of the two planes of symmetry.

Lamb[3] states the following:

> The instantaneous motion of the body at any instant consists, by a well-known theorem of Kinematics, of a twist about a certain screw . . . There are therefore three permanent screw-motions such that the corresponding impulsive wrench in each case reduces to a couple only. The axes of these three screws are mutually at right angles, but do not in general intersect.

To modern ears, the language he uses may sound as torturous as the image it creates, but if the words "axes . . . mutually at right angles, [which] do not in general intersect" are extracted, it can be seen that this is the same idea as multiple centers. In the general case, with no symmetry, we can only define the principal axes, and there is no obvious way to designate a unique point on any axis as a center. In fact, identifying a center is not absolutely necessary, but is only a mathematical convenience.

The purpose of the present paper is to determine simple formulas for finding the various centers in the case of finite thickness and to describe practical means of computing the effect of apparent mass for a typical parafoil.

## Notation

In what follows, several coordinate systems with different origins are utilized, but all such systems have the same orientation, that is, their axes are parallel to the axes of the parafoil. Thus, when a vector is written as a column matrix, there is never any question as to how to translate the vector into three components. This permits us to write everything as a matrix. Lower case bold represents a $3 \times 1$ column matrix. We use a system of notation established by Hughes[13] for the cross product. For any column matrix $\boldsymbol{v}$, the superscript cross represents the cross product matrix:

$$\boldsymbol{v}^{\times} = \begin{bmatrix} 0 & -v_3 & v_2 \\ v_3 & 0 & -v_1 \\ -v_2 & v_1 & 0 \end{bmatrix}$$

The subscripts 1, 2, and 3 are associated with the $x$, $y$, and $z$ axes, respectively. Hughes[13] also uses a convention that $\boldsymbol{I}$ represents the moment of inertia of a body about its center of mass and $\boldsymbol{J}$ represents the moment of inertia about some other point. We follow a similar convention. Finally, we follow the convention established by Lamb[3] that the density is left out of the equations given herein. These equations must be multiplied by density to obtain the dimensionally correct apparent masses and moments of inertia.

## Analysis

For parachute dynamic analysis, it is rarely convenient to make the center of the equations of motion (EOM) the same as one of the centers of apparent mass. A more suitable point may be the center of solid mass. This point has the virtue of being independent of the density of the air, which may be important if there is a desire to simulate a descent through a large change in altitude. If the payload/parachute system is modeled using two-body dynamics, the attachment between the bodies may be the most appropriate EOM center. The result is that there are three points of interest, namely, the roll center, the pitch center, and the EOM as shown in Fig. 2. The subscripts $r$, $p$, and $o$ are used to designate these points.

Let $\boldsymbol{M}$ be the translational part of the apparent inertia matrix:

$$\boldsymbol{M} \equiv \begin{bmatrix} m_{11} & 0 & 0 \\ 0 & m_{22} & 0 \\ 0 & 0 & m_{33} \end{bmatrix} \tag{1}$$

For a body such as a parafoil with lateral symmetry there are at most two off-diagonal terms, in the 13 and 31 positions, that must be equal because it is known that $\boldsymbol{M}$ is symmetric. Because $\boldsymbol{M}$ is also positive definite, it is always possible to choose the orientation of the coordinate frame such that $\boldsymbol{M}$ becomes diagonal, as shown. Let the subscript MC designate the motion center and define

$$\boldsymbol{a}_{\mathrm{MC},o} = \text{vector to MC from} O \tag{2}$$

The phrase momentum of the flow is used herein, even though in a strict sense this is indeterminate. As discussed in Refs. 1 and 3, the integral of pressures over the body leads to variations in momentum that are analogous to the way momentum changes for a solid body. The linear momentum $\boldsymbol{p}$ of the flow may be written

$$\boldsymbol{p} = \boldsymbol{M}\left(\boldsymbol{v}_o + \boldsymbol{\omega}^{\times}\boldsymbol{a}_{\mathrm{MC},o}\right) \tag{3}$$

Different apparent mass effects are obtained depending on the axis of motion. For the momentum in the $x$ direction MC $= p$ must be

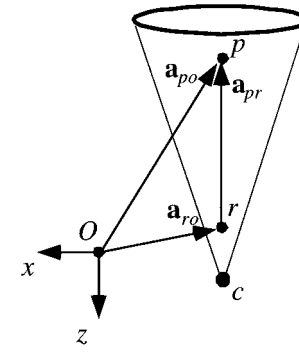


**Fig. 2 Side view of a parafoil, shifted origin.**

substituted, and for the momentum in the $y$ direction MC $= r$ must be substituted. Thus, using scalar components of $\boldsymbol{p}$,

$$p_1 = m_{11}(v_{o1} + \omega_2 a_{po3} - \omega_3 a_{po2})$$

$$p_2 = m_{22}(v_{o2} + \omega_3 a_{ro1} - \omega_1 a_{ro3})$$

$$p_3 = m_{33}(v_{o3} + \omega_1 a_{ro2} - \omega_2 a_{ro1}) \tag{4}$$

where $r$ has been arbitrarily chosen in the third equation, although choosing the subscript $p$ gives the same result. This can be shown by invoking lateral symmetry, which requires

$$a_{po2} = a_{ro2} = 0 \tag{5}$$

and then using fore-and-aft symmetry, which requires

$$a_{ro1} = a_{po1} \tag{6}$$

Using Eq. (5) in Eq. (4) produces

$$p_1 = m_{11}(v_{o1} + \omega_2 a_{po3}) \tag{7}$$

$$p_2 = m_{22}(v_{o2} + \omega_3 a_{ro1} - \omega_1 a_{ro3}) \tag{8}$$

$$p_3 = m_{33}(v_{o3} - \omega_2 a_{ro1}) \tag{9}$$

from which it is evident that using the subscript $p$ in Eq. (9) would not cause any change. These three equations may be combined into the matrix form

$$\boldsymbol{p} = \boldsymbol{M}\left(\boldsymbol{v}_o - \boldsymbol{a}_{ro}^{\times}\boldsymbol{\omega} - \boldsymbol{a}_{pr}^{\times}\boldsymbol{\omega}_2\right) \tag{10}$$

where

$$\boldsymbol{\omega}_2 \equiv [\,0 \quad \omega_2 \quad 0\,]^T \tag{11}$$

This form is justified from the observation that $\boldsymbol{a}_{pr}$ is in the $z$ direction and $\boldsymbol{\omega}_2$ is in the $y$ direction, so that the last term is purely in the $x$ direction. Thus, including this term reproduces Eq. (7), but has no effect on Eqs. (8) or (9). An equally valid expression is obtained by swapping $p$ for $r$ and 1 for 2:

$$\boldsymbol{p} = \boldsymbol{M}\left(\boldsymbol{v}_o - \boldsymbol{a}_{po}^{\times}\boldsymbol{\omega} - \boldsymbol{a}_{rp}^{\times}\boldsymbol{\omega}_1\right) \tag{12}$$

Using elementary unit vectors, $\boldsymbol{\omega}_2$ can be formed via

$$\boldsymbol{\omega}_2 = \boldsymbol{e}_2\boldsymbol{e}_2^T\boldsymbol{\omega} \tag{13}$$

Define

$$\boldsymbol{S}_n \equiv \boldsymbol{e}_n\boldsymbol{e}_n^T \tag{14}$$

Thus, for example,

$$\boldsymbol{S}_2 = \begin{bmatrix} 0 & 0 & 0 \\ 0 & 1 & 0 \\ 0 & 0 & 0 \end{bmatrix} \tag{15}$$

$S_n$ is a selection matrix. It selects component $n$ of any vector and sets the other two components to zero. The matrix form of the momentum becomes, using Eq. (10),

$$\boldsymbol{p} = \boldsymbol{M}\left(\boldsymbol{v}_o - \boldsymbol{a}_{ro}^{\times}\boldsymbol{\omega} - \boldsymbol{a}_{pr}^{\times}\boldsymbol{S}_2\boldsymbol{\omega}\right) \tag{16}$$

Turning now to the angular momentum, the three axes of the "permanent screw-motions" defined by Lamb[3] are, in fact, the principal axes. Define

$$\boldsymbol{I} \equiv \begin{bmatrix} I_{11} & 0 & 0 \\ 0 & I_{22} & 0 \\ 0 & 0 & I_{33} \end{bmatrix} \tag{17}$$

where $I_{nn}$ is the moment of inertia about principal axis $n$. The axes of the coordinate system must be parallel to these principal axes. The origin $O$ is not part of the definition of $\boldsymbol{I}$ and may be located anywhere in the plane of lateral symmetry. Both the roll principal axis and the yaw principal axis must lie in this plane. It is convenient to designate the point where they intersect as both the roll center and the yaw center. An equally valid approach that is used herein is that the roll center is the point along the yaw axis through which the axis of roll rotation must pass if the roll inertia is to assume its minimum value. The pitch center is at the intersection of the pitch principal axis and the plane of lateral symmetry. To summarize, $I_{11}$ will be the value of roll inertia about the roll center, and $I_{22}$ will be the value of pitch inertia about the pitch center. Thus, there is no single reference position for which the rotational inertia matrix equals $\boldsymbol{I}$.

For the simple model analyzed herein, the yaw principal axis coincides with the intersection of two planes of symmetry, and so there is no difficulty determining the location or orientation of the principal axes. Without this second plane of symmetry, this issue would have to be addressed.

A straightforward derivation of a valid expression for the angular momentum proved to be elusive. The most understandable approach is the one actually used by the author; namely, to write down an expression based on what we expect for a rigid body and then modify this to achieve consistency with all requirements. In this vein, the angular momentum about the roll center is a good starting point. If the origin is at $r$, then $\boldsymbol{a}_{ro} = 0$ and $\boldsymbol{v}_o = \boldsymbol{v}_r$. Equation (16) becomes

$$\boldsymbol{p} = \boldsymbol{M}\boldsymbol{v}_r - \boldsymbol{M}\boldsymbol{a}_{pr}^{\times}\boldsymbol{S}_2\boldsymbol{\omega} = \begin{bmatrix}\boldsymbol{M} & -\boldsymbol{M}\boldsymbol{a}_{pr}^{\times}\boldsymbol{S}_2\end{bmatrix}\begin{bmatrix}\boldsymbol{v}_r \\ \boldsymbol{\omega}\end{bmatrix} \tag{18}$$

The angular momentum about $r$ for a rigid body would be

$$\boldsymbol{h}_r = \boldsymbol{I}\boldsymbol{\omega} + \boldsymbol{a}_{pr}^{\times}\boldsymbol{p} \tag{19}$$

By substitution from Eq. (18) and rearrangement,

$$\boldsymbol{h}_r = \boldsymbol{a}_{pr}^{\times}\boldsymbol{M}\boldsymbol{v}_r + \boldsymbol{I}\boldsymbol{\omega} - \boldsymbol{a}_{pr}^{\times}\boldsymbol{M}\boldsymbol{a}_{pr}^{\times}\boldsymbol{S}_2\boldsymbol{\omega} \tag{20}$$

The middle term is correct, and the last term gives a proper accounting for some additional angular momentum being induced when there is a pitching motion, but there is a problem with the first term. The vector $\boldsymbol{a}_{pr}$ only has a $z$ component. Let us represent this scalar value by $a_{pr}$. Then

$$\boldsymbol{a}_{pr}^{\times}\boldsymbol{M}\boldsymbol{v}_r = \begin{bmatrix} 0 & -a_{pr} & 0 \\ a_{pr} & 0 & 0 \\ 0 & 0 & 0 \end{bmatrix}\begin{bmatrix} m_{11}v_{r1} \\ m_{22}v_{r2} \\ m_{33}v_{r3} \end{bmatrix} = \begin{bmatrix} -a_{pr}m_{22}v_{r2} \\ a_{pr}m_{11}v_{r1} \\ 0 \end{bmatrix}$$

The $y$ component of this product is correct because there is pitch angular momentum about $r$ associated with $v_{r1}$. However, the $x$ component should be zero. To correct this problem, the first term in Eq. (20) is premultiplied by $\boldsymbol{S}_2$:

$$\boldsymbol{h}_r = \boldsymbol{S}_2\boldsymbol{a}_{pr}^{\times}\boldsymbol{M}\boldsymbol{v}_r + \boldsymbol{I}\boldsymbol{\omega} - \boldsymbol{a}_{pr}^{\times}\boldsymbol{M}\boldsymbol{a}_{pr}^{\times}\boldsymbol{S}_2\boldsymbol{\omega} \tag{21}$$

Note that now the factor multiplying $\boldsymbol{v}_r$ is the transpose of the factor multiplying $\boldsymbol{\omega}$ in Eq. (18).

What happens if the origin is not at $r$, but at point $O$ in the $x$–$z$ plane? Translation to the new origin can be accomplished using

$$\boldsymbol{v}_r = \boldsymbol{v}_o - \boldsymbol{a}_{ro}^{\times}\boldsymbol{\omega} \tag{22}$$

and

$$\boldsymbol{h}_o = \boldsymbol{h}_r + \boldsymbol{a}_{ro}^{\times}\boldsymbol{p} \tag{23}$$

The analysis proceeds by substituting Eq. (22) into Eq. (21) and using the result plus Eq. (16) in Eq. (23). Along the way it is useful to form the combination $\boldsymbol{Q} \equiv \boldsymbol{S}_2\boldsymbol{a}_{pr}^{\times}\boldsymbol{M}\boldsymbol{a}_{ro}^{\times}$. The result is

$$\boldsymbol{h}_o = \left(\boldsymbol{S}_2\boldsymbol{a}_{pr}^{\times} + \boldsymbol{a}_{ro}^{\times}\right)\boldsymbol{M}\boldsymbol{v}_o + \boldsymbol{J}_o\boldsymbol{\omega} \tag{24}$$

where

$$\boldsymbol{J}_o \equiv \boldsymbol{I} - \boldsymbol{a}_{ro}^{\times}\boldsymbol{M}\boldsymbol{a}_{ro}^{\times} - \boldsymbol{a}_{pr}^{\times}\boldsymbol{M}\boldsymbol{a}_{pr}^{\times}\boldsymbol{S}_2 - \boldsymbol{Q} - \boldsymbol{Q}^T \tag{25}$$

is the inertia matrix about point $O$. The equations may be combined in the form

$$\begin{bmatrix} \boldsymbol{p} \\ \boldsymbol{h}_o \end{bmatrix} = \boldsymbol{A}_o \begin{bmatrix} \boldsymbol{v}_o \\ \boldsymbol{\omega} \end{bmatrix} \tag{26}$$

where the $6 \times 6$ apparent mass matrix is

$$\boldsymbol{A}_o = \begin{bmatrix} \boldsymbol{M} & -M\left(\boldsymbol{a}_{ro}^{\times} + \boldsymbol{a}_{pr}^{\times}\boldsymbol{S}_2\right) \\ \left(\boldsymbol{S}_2\boldsymbol{a}_{pr}^{\times} + \boldsymbol{a}_{ro}^{\times}\right)\boldsymbol{M} & \boldsymbol{J}_o \end{bmatrix} \tag{27}$$

If the origin lies on the line connecting $p$ and $r$, the results simplify. In that case, $\boldsymbol{a}_{po}$, $\boldsymbol{a}_{pr}$, and $\boldsymbol{a}_{ro}$ have the first two components equal to zero. Let $a_{po}$, $a_{pr}$, and $a_{ro}$, respectively, be the scalar values of the third components. Then $\boldsymbol{J}_o$ becomes diagonal with the following values:

$$J_{o11} = I_{11} + a_{ro}^2 m_{22}$$

$$J_{o22} = I_{22} + a_{ro}^2 m_{11} + a_{pr}^2 m_{11} + 2a_{pr}a_{ro}m_{11}$$

$$J_{o22} = I_{22} + a_{po}^2 m_{11}, \qquad J_{o33} = I_{33} \tag{28}$$

The apparent mass matrix becomes

$$\boldsymbol{A}_o = \begin{bmatrix} m_{11} & 0 & 0 & 0 & -m_{11}a_{po} & 0 \\ 0 & m_{22} & 0 & m_{22}a_{ro} & 0 & 0 \\ 0 & 0 & m_{33} & 0 & 0 & 0 \\ 0 & m_{22}a_{ro} & 0 & J_{o11} & 0 & 0 \\ -m_{11}a_{po} & 0 & 0 & 0 & J_{o22} & 0 \\ 0 & 0 & 0 & 0 & 0 & J_{o33} \end{bmatrix} \tag{29}$$

## Apparent Mass Terms for a Flat Wing

The flat wing shown in Fig. 3 was analyzed using the panel code VSAERO.[14] This was modeled using 1600 panels for the main portion plus 160 panels for each tip. A cross section taken in a plane $y =$ constant is an ellipse. A cross section in a plane $x =$ constant shows each wing tip as a semicircle. This wing has the following properties: AR $= 3$, $b = 3$, $c = 1$, and $t = 0.15$.

Because $c = 1$, the chord is the reference length. VSAERO provides results in the form of force and moment coefficients *CFX*, *CFY*, *CFZ*, *CMX*, *CMY*, *CMZ*, for accelerations in translation and rotation along three axes, for a total of 36 coefficients. These must be multiplied by various combinations of the wing dimensions according to the user's manual to get the actual values of apparent mass and inertia.

Lissaman and Brown[1] have provided parametric equations for the apparent mass terms. It is appropriate to begin by examining their formulas for a flat wing. (The term flat is used to mean no spanwise camber.) These are based on the following well-known result for a two-dimensional ellipse:

$$\boldsymbol{M}_{2D} = \pi b \begin{bmatrix} s_y^2 & 0 \\ 0 & s_x^2 \end{bmatrix} \tag{30}$$

where $s_x$ and $s_y$ are the semi-axes in the $x$ and $y$ directions and $b$ is the length perpendicular to the plane of the ellipse. Note that, for motion parallel to $x$ or $y$, the apparent mass depends only on the width of the ellipse perpendicular to the direction of motion. In both cases, it is equal to the mass of air enclosed within a cylinder whose diameter is this width.

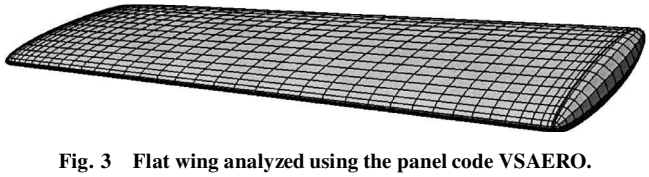

**Fig. 3 Flat wing analyzed using the panel code VSAERO.**

Three-dimensional correction factors are applied to Eq. (30) based on an unpublished work by Adkins. The essence of the approach is to model the flow as that over a comparable spheroid. The derivation goes back to Bateman,[15] who recommended the following for the kinetic energy of the flow:

$$T = \tfrac{4}{3}K\rho S^2 V^2 / l \tag{31}$$

where $S$ is the largest area normal to the flow and $l$ is its perimeter. The parameter $K$ is the linear Bateman coefficient, which is a function of the geometry. The apparent mass is obtained from

$$m = 2T/V^2 \tag{32}$$

Bateman[15] supplies values for $K$ as a function of fineness ratio of the spheroid. For motion in the $x$ direction, the wing is modeled as an oblate spheroid, moving edge on. For motion in the $y$ direction, the wing is modeled as a prolate spheroid with its axis of rotation aligned in the $y$ direction. For motion in the $z$ direction, Adkins finds (unpublished) that for an elliptic wing of sufficiently large aspect ratio, strip theory gives agreement with the solution for an elliptic disk supplied by Lamb. Adkins concludes that strip theory can be used for planforms other than elliptical, as long as the result is put in the form of Bateman.[15] To do this for rectangular wings, Adkins puts (33) into the form

$$m = \tfrac{4}{3}K\rho Sc[b/(l/2)] = \tfrac{4}{3}K\rho Sc[\mathrm{AR}/(\mathrm{AR}+1)] \tag{33}$$

and then chooses the value $K = 3\pi/16$. The ratio of the semiperimeter $(l/2)$ to the span is known as the Jones edge velocity correction (see Ref. 16).

The results quoted by Lissaman and Brown[1] follow. The subscript $f$ denotes flat:

$$m_{f11} = k_A \pi (t^2 b/4) \tag{34}$$

$$m_{f22} = k_B \pi (t^2 c/4) \tag{35}$$

$$m_{f33} = [\mathrm{AR}/(1+\mathrm{AR})]\pi (c^2 b/4) \tag{36}$$

$$I_{f11} = 0.055[\mathrm{AR}/(1+\mathrm{AR})]bS^2 \tag{37}$$

$$I_{f22} = 0.0308[\mathrm{AR}/(1+\mathrm{AR})]c^3 S \tag{38}$$

$$I_{f33} = 0.055 b^3 t^2 \tag{39}$$

According to Ref. 1, these numeric constants are only valid near AR $= 3$. Here, $k_A$ and $k_B$ are correction factors for three-dimensional effects, which can be related to $K$. For the $m_{f11}$ and $m_{f22}$ terms, these factors multiply the volume of a cylinder of the appropriate length and diameter. The value given in Ref. 1 are $k_A = 0.85$ and $k_B = 0.339$. The very low value of $k_B$ is justified by the statement that, "We expect that there will be strong three-dimensional effects, the aspect ratio being low in the side-slip direction...." However, the aspect ratio in the side-slip direction is $c/t = 6.67$, which is actually quite high. It is hard to understand why the three-dimensional correction should be smaller than the factor AR$/(1+$AR$)$ for $m_{f33}$.

A numerical study of $m_{f22}$ for various shapes was undertaken using VSAERO. Defining

$$k_B \equiv 4m_{f22} \big/ \pi t^2 c \tag{40}$$

the following results were obtained: $k_B = 0.33$, ellipsoid with axis ratio 3 to 1 to 0.15; $k_B = 1.00$, wing with ellipsoidal end caps (Fig. 3); $k_B = 1.24$, wing with flat end caps.

Thus, the value of $k_B$ is fairly sensitive to the details of the tip shape. Lissaman and Brown[1] state that "the value of $k$ in each case should be close to, but below, unity." The preceding results show that this is not necessarily true because it is possible that the increase due to bluntness is greater than the decrease due to three-dimensional

**Table 1 Panel code values vs approximation, flat wing**

| Term | VSAERO | Approximation | Equation |
|---|---|---|---|
| $m_{f11}$ | 0.0466 | 0.0449 | (35) |
| $m_{f22}$ | 0.0176 | 0.0177 | (36) |
| $m_{f33}$ | 1.94 | 1.77 | (37) |
| $I_{f11}$ | 1.041 | 1.11 | (38) |
| $I_{f22}$ | 0.0646 | 0.0693 | (39) |
| $I_{f33}$ | 0.0257 | 0.0334 | (40) |

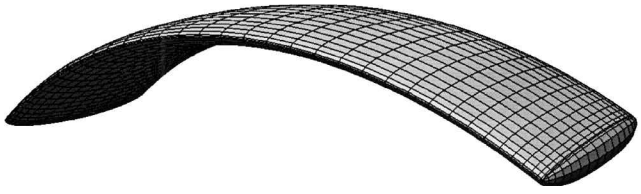

**Fig. 4 Wing of Fig. 3 with spanwise camber.**

effects. By the use of $k_A = 0.85$ and $k_B = 1.0$, numerical results for all six terms are shown in Table 1.

As can be seen, the approximation formulas give values that agree within about 10% with the panel code, except for the last term (the yaw term).

## Estimating Apparent Mass with Spanwise Camber

A parafoil shape was generated by taking the aforementioned flat wing and adding spanwise camber or arch as shown in Figs. 4 and 5. The parameters $t$ and $c$ are the same as before. The reference center (point $O$) was set at the confluence point. The arch is described by

$$R = 2.5 \text{ chords} \tag{41}$$

$$\Theta = 0.611 \text{ rad} (35 \text{ deg}) \tag{42}$$

When an allowance is made for the ellipsoidal end caps at each wing tip, the span of this wing is almost exactly 3. Lissaman and Brown[1] describe the arch in terms the dimension $h$ (which they call $a$), and the ratio $h^* = h/b$. This is approximated by

$$h^* = \frac{R(1-\cos\Theta)}{2R\sin\Theta} \cong \frac{\Theta}{4} \tag{43}$$

When there is spanwise camber, the terms $a_{ro}$ and $a_{po}$ must be estimated, in addition to correcting the six diagonal terms of $\boldsymbol{A}$. It seems reasonable that the pitch center is at the centroid of the arc. The location of the centroid in the reference frame is (Fig. 5)

$$a_{pc} = \pm\frac{\int_{-\Theta}^{\Theta} R^2\cos\theta\,\mathrm{d}\theta}{\int_{-\Theta}^{\Theta} R\,\mathrm{d}\theta} = \pm\frac{R\sin\Theta}{\Theta} \tag{44}$$

The subscript $c$ designates the confluence point and the notation $a_{pc}$ should be read as the location of the pitch center relative to $c$. This is a fixed parameter of the canopy, as opposed to $a_{po}$, which varies according to the location of point $O$. The correct sign depends on whether the positive $z$ axis of the reference frame is defined as up or down.

To compute $a_{rc}$, a few conjectures are necessary. For roll motion about the confluence point, it can be expected that there will be some flow disturbance due to thickness at the left tip and a mirror-image disturbance at the right tip. Not much is happening in the middle. The same kind of flow will occur for the flat wing in the case of translation in the $y$ direction. Therefore, the forces required to accelerate the flow will be the same. This leads to the first conjecture:

$$J_{c11} = R^2 m_{f22} \tag{45}$$

where it is emphasized that this is a relationship between a flat wing with lateral motion and an arched wing rolling about its confluence

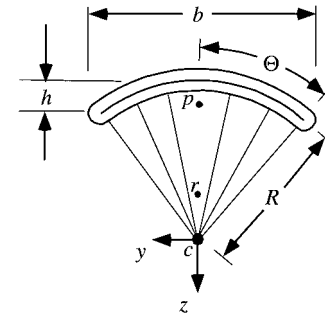


**Fig. 5 Front view of arched parafoil.**

point $c$. The VSAERO results confirm this equation to three decimal places.

The second conjecture is that the roll inertia for motion about the centroid is not affected by arch or thickness. This is in line with the procedure used by Lissaman and Brown.[1] In discussing the roll inertia, they state that "We make no correction for thickness or arch effect."[1] In mathematical terms, this becomes

$$J_{\text{cen}11} = I_{f11} \tag{46}$$

where a flat wing is now being compared to an arched wing rotating about the centroid of its arc. $J$ is used for the arched wing because its centroid is not at its roll center, and $I$ is used for the flat wing, which is rolling about its roll center.

Let the reference point move up or down by a distance $z$, and define

$$\bar{z} \equiv z/a_{pc} \tag{47}$$

Note that this eliminates any sign ambiguity; $\bar{z}$ will be positive when the reference point is above the confluence point, even if the positive $z$ axis is down. The third conjecture is that the roll inertia is composed of a thickness effect and a normal motion effect. Imagine a segment of the arc that is short enough to be approximated by a line. Normal motion is defined as any motion normal to this line. There is no normal motion effect when the reference point is at the confluence point ($\bar{z} = 0$) and no thickness effect when the reference point is at the centroid ($\bar{z} = 1$). We express this as follows:

$$J_{11} = (\bar{z}-1)^2 R^2 m_{f22} + \bar{z}^2 I_{f11} \tag{48}$$

where the first term is the thickness effect and the second term is the normal motion effect. This equation has been crafted to agree with both Eqs. (45) and (46) and to avoid negative contributions from either term. It is a straightforward matter to set the derivative of this expression to zero to find the value of $\bar{z}$ corresponding to the minimum roll inertia:

$$\bar{z}_{\min} = \frac{R^2 m_{f22}}{R^2 m_{f22} + I_{f11}} \tag{49}$$

This gives the location of the roll center. Equation (48) can be used to obtain

$$a_{rc} = z_{\min} = \frac{a_{pc} m_{f22}}{m_{f22} + I_{f11}/R^2} \tag{50}$$

The next step is to correct the six diagonal terms of $\boldsymbol{A}$. Following Ref. 1, the $m_{11}$ term can be obtained from Eq. (34) by using the arc length of the wing instead of the horizontal span. We first approximate the ratio (arc length/$b$) in terms of $\Theta$ and then use Eq. (43) to get

$$m_{11} = k_A\left[1 + \left(\tfrac{8}{3}\right)h^{*2}\right]\pi(t^2 b/4) \tag{51}$$

To compute the sideslip term $m_{22}$, it is reasoned that in the limit as $z \to \infty$ the parallel axis theorem gives

$$J_{11} \to z^2 m_{22}$$

whereas Eq. (48) gives

$$J_{11} \to z^2\left(R^2 m_{f22} + I_{f11}\right)/a_{pc}^2$$

thus

$$m_{22} = \left(R^2 m_{f22} + I_{f11}\right)/a_{pc}^2 \tag{52}$$

If the VSAERO values from Table 1 are inserted into this expression, the error is less than 2%.

The correction in Ref. 1 for the combined effect of arch and thickness on $m_{33}$ is very small and may be of the wrong sign. The VSAERO results indicate that the arched span has a value of $m_{33}$, which is less than, rather than greater than, that for the flat span. The difference between flat and arched is only 2%, which may be within the range of accuracy of the numerical results. It seems a contradiction to state that $m_{33}$ depends on the amount of arch but that $J_{\text{cen}11}$ does not, and so Eq. (36) should be accepted unchanged for an arched span.

The roll inertia about the roll center is obtained by substituting $\bar{z}_{\min} = a_{rc}/a_{pc}$ into Eq. (48) and simplifying

$$I_{11} = \left(a_{pr}^2/a_{pc}^2\right)R^2 m_{f22} + \left(a_{rc}^2/a_{pc}^2\right)I_{f11} \tag{53}$$

There is no corresponding inertia term from Ref. 1. The variation of roll inertia with $R/b$ is shown in Fig. 6. The minimum value of $R/b$ plotted in this graph, 1/2, corresponds to the extreme case of a semicircular wing (not realistic for a parafoil).

The arch and thickness correction in Ref. 1 for $I_{22}$ is truly miniscule and can be ignored. Thus, the pitch inertia about the pitch center is

$$I_{22} = I_{f22} \tag{54}$$

Finally, we have the yaw term. In Ref. 1 the following expression is suggested:

$$I_{33} = 0.055(1 + 8h^{*2})b^3 t^2 \tag{55}$$

This happens to agree rather well with the VSAERO results for the present set of parameters, which may be fortuitous because poor agreement was obtained from this same expression for the case of a flat wing. Note that this is the smallest rotational inertia term, and even though the approximation may not be as accurate if the parameters are changed, this term is likely to be small compared to the yaw inertia from the combined effect of the solid mass term and the enclosed air mass. Thus, improvements to the yaw approximation are probably not necessary.

Comparisons of all of these formulas with numerical results are shown in Table 2. The parameters $a_{pc}$ and $a_{rc}$ were obtained from the numerical results by observing from Eq. (29) that if the origin $O$ is the confluence point $c$, then

$$a_{pc} = -\boldsymbol{A}_{c15}/\boldsymbol{A}_{c11} \tag{56}$$

$$a_{rc} = \boldsymbol{A}_{c24}/\boldsymbol{A}_{c22} \tag{57}$$

These ratios give the centers in terms of the reference length (the chord).

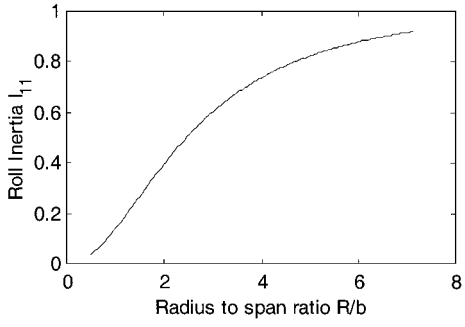


**Fig. 6 Roll inertia about the roll center vs radius to span ratio, AR = 3**

**Table 2 Panel code values vs approximation, arched wing**

| Term | VSAERO | Approximation | Equation |
|---|---|---|---|
| $m_{11}$ | 0.0503 | 0.0478 | (52) |
| $m_{22}$ | 0.206 | 0.221 | (53) |
| $m_{33}$ | 1.90 | 1.77 | (37) |
| $I_{11}$ | 0.104 | 0.100 | (54) |
| $I_{22}$ | 0.0624 | 0.0693 | (39) |
| $I_{33}$ | 0.0379 | 0.0395 | (56) |
| $a_{pc}$ | 2.38 | 2.35 | (57), (45) |
| $a_{rc}$ | 0.172 | 0.215 | (58), (51) |

## Dynamic Equations

The most illuminating approach to the dynamic equations is to include the real mass, in addition to the apparent mass. Thus, a subscript $a$ is attached to the apparent momenta and inertia matrices to distinguish them from the real mass terms:

$$\boldsymbol{p} \to \boldsymbol{p}_a, \qquad \boldsymbol{h}_o \to \boldsymbol{h}_{oa}$$

$$\boldsymbol{M} \to \boldsymbol{M}_a, \qquad \boldsymbol{A}_o \to \boldsymbol{A}_{oa}$$

Then we can write

$$\dot{\boldsymbol{p}}_t = \dot{\boldsymbol{p}}_R + \dot{\boldsymbol{p}}_a = \boldsymbol{f}_{\text{aero}} + \boldsymbol{f}_e + \boldsymbol{f}_{R\,\text{nl}} + \boldsymbol{f}_{a\,\text{nl}} \tag{58}$$

The aerodynamic force term $\boldsymbol{f}_{\text{aero}}$ is the force derived from traditional coefficients and stability derivatives. For normal parafoil analyses, the only external force is that due to gravity, which must be expressed in the body frame.

The nonlinear aerodynamic forces are those due to products of the motion variables $\boldsymbol{\omega}$ and $\boldsymbol{v}_o$. They arise from exactly the same considerations as their real mass, that is, rigid-body, counterparts. They may appear unfamiliar because normally the real mass equations are only seen after several steps of simplification, steps that can not be applied to the aerodynamic nonlinearities. A derivation of the rigid-body equations using the present notation appears in Ref. 13. The terms real mass and solid mass are not identical, the difference being the enclosed air mass. The inertia matrix for the real mass is

$$\boldsymbol{A}_{oR} = \begin{bmatrix} m_R \boldsymbol{I} & -m_R \boldsymbol{r}^{\times} \\ m_R \boldsymbol{r}^{\times} & \boldsymbol{J}_{oR} \end{bmatrix} \tag{59}$$

where $\boldsymbol{I}$ is the $3 \times 3$ identity matrix. This expression when expanded becomes the same as Eq. (9) of Thomasson.[5] The nonlinear forces are, using Eq. (16) for $\boldsymbol{p}_a$ and Eq. (59) plus the analog of Eq. (26) for $\boldsymbol{p}_R$,

$$\boldsymbol{f}_{R\,\text{nl}} = \boldsymbol{\omega}^{\times}\boldsymbol{p}_R = \boldsymbol{\omega}^{\times} m_R(\boldsymbol{v}_o - \boldsymbol{r}^{\times}\boldsymbol{\omega}) \tag{60}$$

$$\boldsymbol{f}_{a\,\text{nl}} = \boldsymbol{\omega}^{\times}\boldsymbol{p}_a = \boldsymbol{\omega}^{\times}\boldsymbol{M}_a(\boldsymbol{v}_o - \boldsymbol{D}\boldsymbol{\omega}) \tag{61}$$

where $\boldsymbol{D} = \boldsymbol{a}_{ro}^{\times} + \boldsymbol{a}_{pr}^{\times}\boldsymbol{S}_2$. Note that $\boldsymbol{D}$ is not skew symmetric and can not be written as the cross product of any vector. The angular momentum about $O$ shows a similar development. With $\boldsymbol{g}$ torque and the same subscripts used as for $\boldsymbol{p}$,

$$\dot{\boldsymbol{h}}_{ot} = \dot{\boldsymbol{h}}_{oR} + \dot{\boldsymbol{h}}_{oa} = \boldsymbol{g}_{\text{aero}} + \boldsymbol{g}_e + \boldsymbol{g}_{R\,\text{nl}} + \boldsymbol{g}_{a\,\text{nl}} \tag{62}$$

$$\boldsymbol{g}_{R\,\text{nl}} = -\boldsymbol{v}_o^{\times}\boldsymbol{p}_R - \boldsymbol{\omega}^{\times}\boldsymbol{h}_{oR} \tag{63}$$

$$\boldsymbol{g}_{a\,\text{nl}} = -\boldsymbol{v}_o^{\times}\boldsymbol{p}_a - \boldsymbol{\omega}^{\times}\boldsymbol{h}_{oa} \tag{64}$$

The angular momentum $\boldsymbol{h}_{oa}$ is obtained from Eq. (24), and $\boldsymbol{h}_{oR}$ is obtained from Eq. (59),

$$\boldsymbol{g}_{R\,\text{nl}} = -\boldsymbol{v}_o^{\times} m_R(\boldsymbol{v}_o - \boldsymbol{r}^{\times}\boldsymbol{\omega}) - \boldsymbol{\omega}^{\times} m_R \boldsymbol{r}^{\times}\boldsymbol{v}_o - \boldsymbol{\omega}^{\times}\boldsymbol{J}_{oR}\boldsymbol{\omega} \tag{65}$$

$$\boldsymbol{g}_{a\,\text{nl}} = -\boldsymbol{v}_o^{\times}\boldsymbol{M}_a(\boldsymbol{v}_o - \boldsymbol{D}\boldsymbol{\omega}) + \boldsymbol{\omega}^{\times}\boldsymbol{M}_a\boldsymbol{D}^T\boldsymbol{v}_o - \boldsymbol{\omega}^{\times}\boldsymbol{J}_{oa}\boldsymbol{\omega} \tag{66}$$

The first terms in both of these expressions can be deleted, for different reasons. In the case of the real mass, $\boldsymbol{v}_o^{\times} m_R \boldsymbol{v}_o$ is zero because

it is the cross product of parallel vectors. In the case of the apparent mass, $\boldsymbol{v}_o^{\times}\boldsymbol{M}_a\boldsymbol{v}_o$ is a steady-state term that will normally be included as part of the aerodynamic torque $\boldsymbol{g}_{\text{aero}}$, and it must be deleted from the preceding expression to avoid double counting. For the real mass, the second and third terms may be consolidated using a well-known identity for the triple vector product. Caution must be exercised with the remaining terms for the apparent mass because it is possible that they, too, are included as part of $\boldsymbol{g}_{\text{aero}}$. If the dynamic derivatives such as roll damping are obtained from simple theories, such as strip theory, then there is no such inclusion. On the other hand, a sophisticated computational fluid dynamics program for producing dynamic derivatives might include these apparent mass effects. Reference 1 has an example showing how $m_{33}$ may be part of the dynamic derivative $C_{L_{\dot{\alpha}}}$. One approach to separating the effects is to confine $\boldsymbol{f}_{\text{aero}}$ and $\boldsymbol{g}_{\text{aero}}$ to be the forces and torques that either arise from vorticity or can be measured in a wind tunnel.

The final forms of the nonlinear torque terms become

$$\boldsymbol{g}_{R\,\text{nl}} = m_R\boldsymbol{r}^{\times}\boldsymbol{v}_o^{\times}\boldsymbol{\omega} - \boldsymbol{\omega}^{\times}\boldsymbol{J}_{oR}\boldsymbol{\omega} \tag{67}$$

$$\boldsymbol{g}_{a\,\text{nl}} = \boldsymbol{v}_o^{\times}\boldsymbol{M}_a\boldsymbol{D}\boldsymbol{\omega} + \boldsymbol{\omega}^{\times}\boldsymbol{M}_a\boldsymbol{D}^T\boldsymbol{v}_o - \boldsymbol{\omega}^{\times}\boldsymbol{J}_{oa}\boldsymbol{\omega} \tag{68}$$

The dynamic equations become, using Eqs. (27) and (59)

$$\begin{bmatrix}\dot{\boldsymbol{v}}_o\\ \dot{\boldsymbol{\omega}}\end{bmatrix} = [\boldsymbol{A}_{oR} + \boldsymbol{A}_{oa}]^{-1}\begin{bmatrix}\boldsymbol{f}_{\text{aero}} + \boldsymbol{f}_e + \boldsymbol{f}_{R\,\text{nl}} + \boldsymbol{f}_{a\,\text{nl}}\\ \boldsymbol{g}_{\text{aero}} + \boldsymbol{g}_e + \boldsymbol{g}_{R\,\text{nl}} + \boldsymbol{g}_{a\,\text{nl}}\end{bmatrix} \tag{69}$$

The motion variables $\boldsymbol{v}_o$ and $\boldsymbol{\omega}$ can be integrated in this form. The conversion of these variables into aerodynamic variables such as angle of attack and sideslip is given in many texts, for example, Ref. 17.

## Conclusions

The notion is well-established that the kinetic energy of the fluid surrounding a body makes this body behave as if it has additional apparent mass and an apparent moment of inertia with three principal axes. If there is a plane of symmetry, it turns out to be useful to carry this artifice a bit further and postulate that the three principal axes of motion each have a center in this plane. These centers have similarities to, and differences from, the center of mass that we associate with a rigid body. No single center can be found that eliminates coupling between rotation and translation. Some modification of the usual matrix–vector technique for rigid-body dynamics is required to cope with this situation. The present system of notation allows an easy manipulation of the nonlinear torque terms and avoids what would be a very tedious derivation if done in expanded form.

For parachute roll motions about a point near the confluence point of the suspension lines, the effect of the apparent roll inertia may be greatly reduced by spanwise camber. The authors of Ref. 1, using a wing model with no spanwise camber (a flat wing), concluded that the apparent roll inertia may be as much as five times the solid mass roll inertia. The present analysis concludes that the roll inertia of a cambered wing about the roll center may be as small as 0.1 of the corresponding value for a flat wing (Table 1 vs Table 2). The result is that the roll acceleration is much greater than expected from a flat-wing model. Steady-state turn rates may also be altered from the flat-wing results, but not as dramatically.

A fully populated apparent inertia matrix has 36 terms, of which only 21 are distinct because it must be symmetric. If the body has both lateral and fore-and-aft symmetry, there are only eight fundamental parameters of apparent inertia, as given in Table 2. Given these parameters, for any particular location of the origin the apparent inertia matrix can be computed using Eqs. (25–27).

The present paper is based entirely on potential flow analysis, and no account has been taken of the manner in which the presence of vortices may alter the kinetic energy of the flow.

Whoever stated that a little bit of knowledge is a dangerous thing could have had apparent mass in mind. Lesson number one on the subject is usually that the apparent mass of a circular cylinder is equal to the mass of the fluid displaced by the cylinder, which creates the impression that apparent mass is proportional to volume. This initial lesson has prompted at least one parafoil researcher to use the mass of the enclosed air as a substitute for the diagonal terms of $\boldsymbol{M}$. This impression is corrected by lesson number two, the elliptical cylinder, which teaches us that the dimension in the streamwise direction is irrelevant and that only the dimension perpendicular to the stream matters. This in turn is corrected when we move beyond two-dimensional flow to axisymmetric flow and learn that a disc has greater apparent mass than a sphere of the same radius. Thus, if the flow is three-dimensional, stretching things out in the streamwise direction can cause a decrease in the apparent mass. However, this is not complete. Going back to two-dimensional flow, we find that stretching a circular cylinder into an oval with semicircular ends will increase the apparent mass. No doubt the next researcher will find an example to further refine whatever impression one might glean from that.

## References


[1] Lissaman, P. B. S., and Brown, G. J., "Apparent Mass Effects on Parafoil Dynamics," AIAA Paper 93-1236, 1993.

[2] Brown, G. J., "Parafoil Steady Turn Response to Control Input," AIAA Paper 93-1241, 1993.

[3] Lamb, H., *Hydrodynamics*, Dover, New York, 1945, pp. 154 and 171.

[4] "Study of Ground Handling Characteristics of a Maritime Patrol Airship," Goodyear Aerospace Corp., NASA-CR-166253, March 1981.

[5] Thomasson, P. G., "Equations of Motion of a Vehicle in a Moving Fluid," *Journal of Aircraft*, Vol. 37, No. 4, 2000, pp. 630–639.

[6] Yavuz, T., "Determining and Accounting for a Parachute Virtual Mass," *Journal of Aircraft*, Vol. 26, No. 5, 1989, pp. 432–437.

[7] Cockrell, D. J., and Haidar, N. I. A., "Influence of the Canopy-Payload Coupling on the Dynamic Stability in Pitch of a Parachute System," AIAA Paper 93-1248, 1993.

[8] Doherr, K.-F., "Theoretical and Experimental Investigation of Parachute-Load-System Dynamic Stability," AIAA Paper 75-1397, 1975.

[9] Cockrell, D. J., and Doherr, K.-F., "Preliminary Considerations of Parameter Identification Analysis from Parachute Aerodynamic Flight Test Data," AIAA Paper 81-1940, 1981.

[10] Doherr, K.-F., and Saliaris, C., "Influence of Stochastic and Acceleration Dependent Aerodynamic Forces on the Dynamic Stability of Parachutes," AIAA Paper 81-1941, 1981.

[11] Eaton, J. A., "Added Mass and the Dynamic Stability of Parachutes," *Journal of Aircraft*, Vol. 19, No. 5, 1982, pp. 414–416.

[12] Iosilevskii, G., "Lifting Line Theory of an Arched Wing in Asymmetric Flight," *Journal of Aircraft*, Vol. 33, No. 5, 1996, pp. 1023–1026.

[13] Hughes, P. C., *Spacecraft Attitude Dynamics*, Wiley, New York, 1986, pp. 51–59.

[14] Nathman, J. K., "Subsonic Panel Methods—Second (Order) Thoughts," Society of Automotive Engineers Paper SAE 985563, Sept. 1998.

[15] Bateman, H., "The Inertia Coefficients of an Airship in a Frictionless Fluid," NACA Rept. 164, 1923, pp. 3–16.

[16] Abbott, I., and Von Doenhoff, A., *Theory of Wing Sections*, Dover, New York, 1959, pp. 11 and 25.

[17] Etkin, B., *Dynamics of Atmospheric Flight*, Wiley, New York, 1972, pp. 113–117.